Journal of Oceanology and Limnology
Vol. 36 No. 5, P. 1494-1508, 2018
https://doi.org/10.1007/s00343-018-7077-x

An improved dual-polarized ratio algorithm for sea ice concentration retrieval from passive microwave satellite data and inter-comparison with ASI, ABA and NT2*

ZHANG Shugang (张树刚)[1, 2, **], ZHAO Jinping (赵进平)[2], LI Min (李民)[1],
LIU Shixuan (刘世萱)[1], ZHANG Shuwei (张曙伟)[1]

[1] *Institute of Oceanographic Instrumentation, Shandong Academy of Sciences, Qingdao 266001, China*
[2] *College of Physical and Environmental Oceanography, Ocean University of China, Qingdao 266100, China*

Received Mar. 15, 2017; accepted in principle May 27, 2017; accepted for publication Sep. 19, 2017

Abstract The dual-polarized ratio algorithm (DPR) for the retrieval of Arctic sea ice concentration from Advanced Microwave Scanning Radiometer-EOS (AMSR-E) data was improved using a contrast ratio (CR) parameter. In contrast to three other algorithms (Artist Sea Ice algorithm, ASI; NASA-Team 2 algorithm, NT2; and AMSR-E Bootstrap algorithm, ABA), this algorithm does not use a series of tie-points or a priori values of brightness temperature of sea-ice constituents, such as open water and 100% sea ice. Instead, it is based on a ratio (α) of horizontally and vertically polarized sea ice emissivity at 36.5 GHz, which can be automatically determined by the CR. α exhibited a clear seasonal cycle: changing slowly during winter, rapidly at other times, and reaching a minimum during summer. The DPR was improved using a seasonal α. The systematic differences in the Arctic sea ice area over the complete AMSR-E period (2002–2011) were -0.8%±2.0% between the improved DPR and ASI; -1.3%±1.7% between the improved DPR and ABA; and -0.7%±1.9% between the improved DPR and NT2. The improved DPR and ASI (or ABA) had small seasonal differences. The seasonal differences between the improved DPR and NT2 decreased, except in summer. The improved DPR identified extremely low ice concentration regions in the Pacific sector of the central Arctic (north of 83°N) around August 12, 2010, which was confirmed by the Chinese National Arctic Research Expedition. A series of high-resolution MODIS images (250 m×250 m) of the Beaufort Sea during summer were used to assess the four algorithms. According to mean bias and standard deviations, the improved DPR algorithm performed equally well with the other three sea ice concentration algorithms. The improved DPR can provide reasonable sea ice concentration data, especially during summer.

Keyword: Arctic sea ice; sea ice concentration; algorithm; time series; Advanced Microwave Scanning Radiometer-EOS (AMSR-E)

1 INTRODUCTION

Sea ice covers a significant fraction (5% to 8%) of the oceans and is one of the most important parameters in the global climate system (Liu et al., 2004; Sumata et al., 2015; Nakamura et al., 2016). The results from microwave satellite observations have shown that the Arctic sea ice has been retreating at a higher rate during 1997–2014 than 1979–1997 (Hebert et al., 2015; Serreze and Stroeve, 2015). The IPCC's Fifth Assessment Report indicates that sea ice will vanish by September, 2100 (Stocker et al., 2013). Clearly, model results overestimate minimum sea ice extent because certain physical processes and parameters are not fully understood to accurately predict the state of the Arctic ice pack, such as sea ice concentration, sea ice temperature, and melt ponds (Webster et al., 2015).

* Supported by the National Natural Science Foundation of China (No. 41406208), the Global Change Research of National Important Research Project on Science (No. 2015CB953900), the Scientific and Youth Science Funds of Shandong Academy of Sciences, China (No. 2013QN042), and the Open Research Fund of the State Oceanic Administration of the People's Republic of China Key Laboratory for Polar Science (No. 3KP201203)
** Corresponding author: zhangshugang6@163.com

Table 1 Gridded sea ice concentration and brightness temperature of AMSR-E

Parameter	Footprint size (km^2)	Grid resolution (km^2)
TB (H and V POL.)		
6.9 GHz	43×75	25.0×25.0
10.7 GHz	29×51	25.0×25.0
18.7 GHz	16×27	25.0×25.0, 12.5×12.5
23.8 GHz	18×32	25.0×25.0, 12.5×12.5
36.5 GHz	8.2×14.4	25.0×25.0, 12.5×12.5
89.0 GHz	3.5×5.9	25.0×25.0, 12.5×12.5, 6.25×6.25
Arctic sea ice conc.		
NASA Team2 (NSIDC)		25.0×25.0, 12.5×12.5
ABA (NSIDC)		25.0×25.0, 12.5×12.5
ASI (University of Bremen)		6.25×6.25

Because the microwave signal is independent of daylight and less affected by clouds and weather conditions, microwave satellite observations have become useful tools for monitoring sea ice (Maaβ and Kaleschke, 2010; Stroeve et al., 2016), for example, data from the Special Sensor Microwave/Imager (SSM/I, 1987–to present), the Advanced Microwave Scanning Radiometer-EOS (AMSR-E, 2002–2011), and the Advanced Microwave Scanning Radiometer 2 (AMSR2, 2012–to present). AMSR-E is a twelve channel, six frequency total power passive microwave radiometer system. It measures polarized radiance vertically (V) and horizontally (H) at 6.925, 10.65, 18.7, 23.8, 36.5, and 89.0 GHz.

Sea ice concentration is the principal quantitative sea ice parameter that is measured routinely from microwave satellite observation systems. Sea ice concentration derived from AMSR-E is calculated using the Artist Sea Ice algorithm (ASI) (Spreen et al., 2008), the AMSR-E Bootstrap algorithm (ABA) (Comiso and Zwally, 1997; Comiso et al., 2003), and the NASA-Team 2 algorithm (NT2) (Markus and Cavalieri, 2000; Comiso et al., 2003). NT2 and ABA derive the sea ice concentration from the combination of the V18.7 and V36.5 GHz channels. The National Snow and Ice Data Center (NSIDC) provides sea ice concentration products from NT2 and ABA. The footprint sizes of the 18.7 GHz and 36.5 GHz channels are 16×27 km^2 and 8.2×14.4 km^2, respectively. The different resolution of the channel data causes considerable errors in the sea ice concentration products. ABA and NT2 require more accurate tie-points to measure the sea ice concentration (Comiso and Zwally, 1997; Markus and Cavalieri, 2000; Zhang et al., 2013). ASI estimates sea ice concentration from the 89.0 GHz channels (footprint size: 3.5×5.9 km^2), and the corresponding sea ice concentration products are published by the University of Bremen. The spatial resolution of sea ice concentration derived using ASI is improved because of the footprint size. However, the 89.0 GHz information is more sensitive to atmospheric influence, which restricts ASI application (Andersen et al., 2007; Spreen et al., 2008; Maaβ and Kaleschke, 2010). In addition, ASI uses two priori fixed coefficients for open water and 100% sea ice concentration (Spreen et al., 2008).

Zhang et al. (2013) developed a simple dual-polarized ratio algorithm (DPR) to estimate sea ice concentration from AMSR-E using channels at 36.5 GHz. The core parameter of DPR is the ratio (α) of dual-polarized sea ice emissivity, which is assumed to be a constant value (α=0.92) in all years. We defined the original DPR as α equal to 0.92 in all years. Although the original DPR consistently provided the best agreement with MODIS ice concentration in winter, spring, and autumn, the original DPR results were substantially less than MODIS, NT2, and ABA during summer. The objectives of this study were: (1) to improve the original DPR algorithm by introducing a new technique, which we called the improved DPR; (2) to evaluate the improved DPR algorithm with ship observation and MODIS data; and (3) to compare the four Arctic sea ice concentration datasets (including the improved DPR, ASI, ABA, and NT2) from AMSR-E.

2 DATA AND METHOD

2.1 Dataset

We applied gridded sea ice products (including sea ice concentration and brightness temperatures) derived from AMSR-E (Table 1). The H and V 36.5 GHz channels were used in the original (and improved) DPR to calculate the sea ice concentration. The V18.7 GHz, V23.8 GHz, and V36.5 GHz channels were used as weather filters to exclude high cloud liquid water and high water vapor cases. Sea ice concentration from ASI, ABA, and NT2 were primarily used to compare with the original (and improved) DPR. We also applied ship observations and MODIS images (Band 2, 841–876 nm) to provide independent references to validate the four different algorithms.

The AMSR-E products were on a 12.5×12.5 km^2 grid; the sea ice concentration from ASI and MODIS

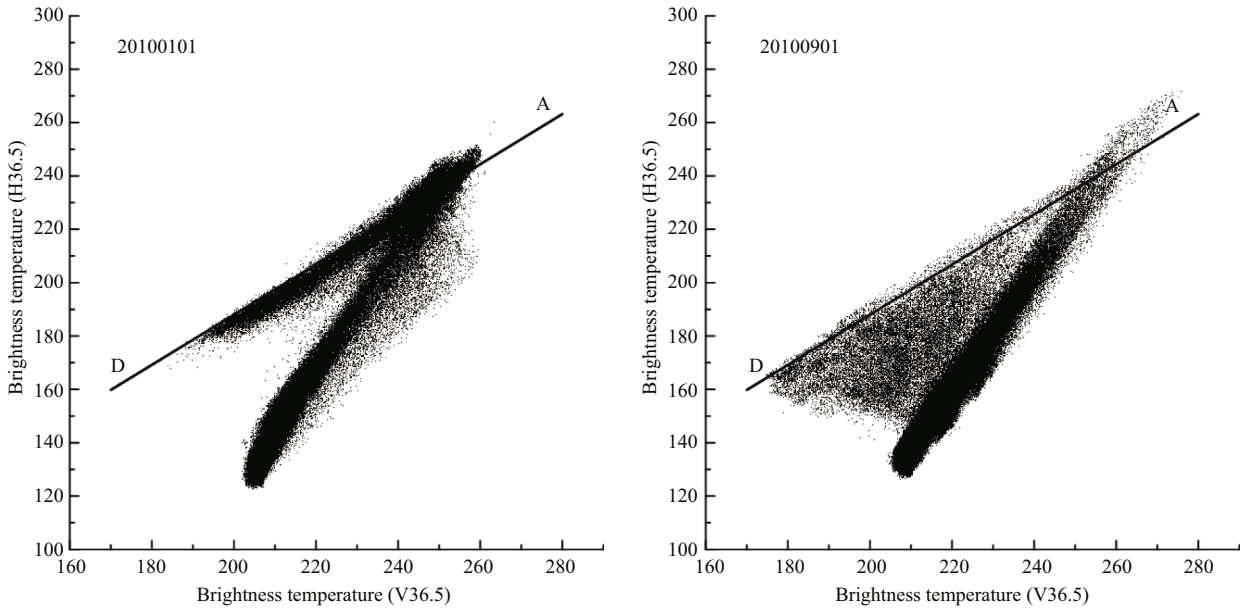

Fig.1 Scatter plots of the dual-polarized brightness temperature at 36.5 GHz derived from AMSR-E in January and September, 2010

The slope of line AD is 0.92.

was gridded to 12.5×12.5 km^2; and MODIS images were obtained on four days (July 22, 23, 24, and 28, 2010) for sea ice changes in the Beaufort Sea.

2.2 Theory of the original DPR

Within the ice pack, the brightness temperature (TB) observed by AMSR-E comes from the sea ice surface, ice-free water, or a combination of both. According to the linear mixing formulation, TB from each gridded net is given by (Comiso et al., 2003)

$$\mathrm{TB}=\varepsilon_\mathrm{I}T_\mathrm{I}C+\varepsilon_\mathrm{W}T_\mathrm{W}(1-C), \quad (1)$$

where C is ice concentration, T_W and T_I are the physical temperatures of open water and sea ice, and ε_I and ε_W are the microwave emissivity of sea ice and open water, respectively.

According to Eq.1, the brightness temperatures of the same frequency are given by

$$\mathrm{TB_V}=\varepsilon_\mathrm{IV}T_\mathrm{I}C+\varepsilon_\mathrm{WV}T_\mathrm{W}(1-C), \quad (2a)$$

$$\mathrm{TB_H}=\varepsilon_\mathrm{IH}T_\mathrm{I}C+\varepsilon_\mathrm{WH}T_\mathrm{W}(1-C). \quad (2b)$$

The sea ice concentration can be estimated from Eq.2:

$$C=1-\frac{\varepsilon_\mathrm{IH}\mathrm{TB_V}-\varepsilon_\mathrm{IV}\mathrm{TB_H}}{T_\mathrm{W}(\varepsilon_\mathrm{IH}\varepsilon_\mathrm{WV}-\varepsilon_\mathrm{IV}\varepsilon_\mathrm{WH})},$$

$$C=1-\frac{\alpha\mathrm{TB_V}-\mathrm{TB_H}}{T_\mathrm{W}(\alpha\varepsilon_\mathrm{WV}-\varepsilon_\mathrm{WH})}, \quad (3)$$

where $\alpha=\varepsilon_\mathrm{IH}/\varepsilon_\mathrm{IV}$. In the original DPR, the dual-polarized brightness temperatures of 36.5 GHz (H and V36.5 GHz) were used in Eq.3. Scatter plots using H and V36.5 GHz are shown in Fig.1 for January and September, 2010. In these plots, the cluster of data dots along line AD represent 100% sea ice concentration (Comiso et al., 2003). Therefore, for consolidated (100%) ice, α can be written as

$$\alpha=\frac{\varepsilon_\mathrm{IH}}{\varepsilon_\mathrm{IV}}=\frac{\varepsilon_\mathrm{IH}T_\mathrm{I}}{\varepsilon_\mathrm{IV}T_\mathrm{I}}=\frac{\mathrm{TB_H}}{\mathrm{TB_V}}. \quad (4)$$

Equation 4 indicates that α is the slope of line AD. The cluster of data dots in Fig.1 also show that the α (or the slope of line AD) is almost a constant. The original DPR algorithm uses 0.92 as the slope of line AD (or α=0.92) in all years (Zhang et al., 2013).

To remove, or greatly reduce, spurious ice concentration in open water areas, the original DPR employs three steps of weather filtering. First, the weather filter uses the gradient ratio of the V36.5 and V18.7 GHz channels, called GR (36.5/18.7), to cut off all spurious ice (Gloersen and Cavalieri, 1986; Spreen et al., 2008). The ice concentration for each GR (36.5/18.7) greater than 0.045 is set to zero. Second, the gradient ratio GR (23.8/18.7) is used to exclude high water vapor. When GR (23.8/18.7) is greater than 0.04, the ice concentration is set to zero. Third, all original DPR results with corresponding NT2 equal to zero are set to zero.

Because open water inside the ice pack normally has a smooth surface, ε_WH and ε_WV can be determined by the emissivity of calm sea water (Svendsen et al.,

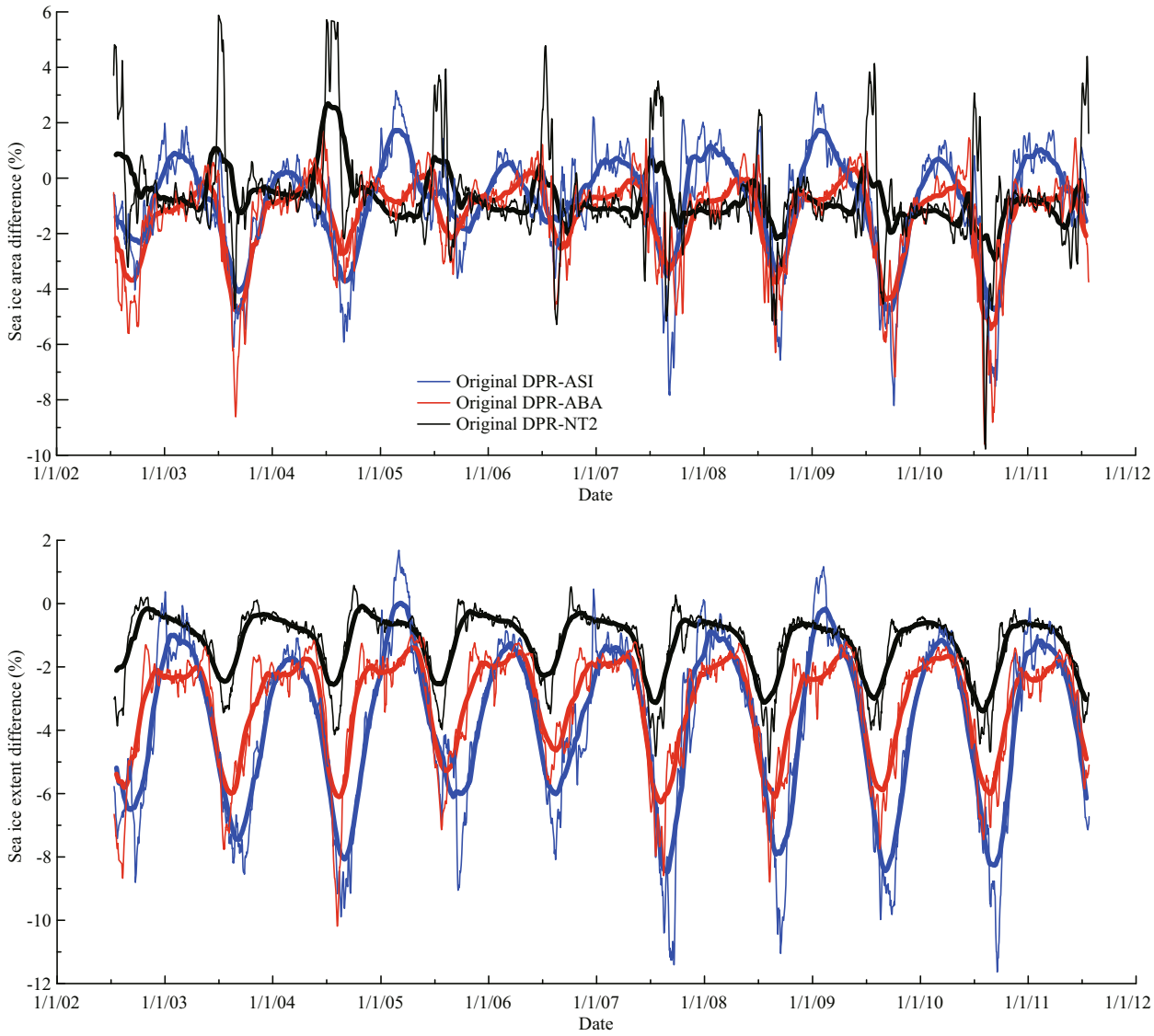

Fig.2 Time series of the differences in Arctic sea ice area (top) and extent (bottom)

The thick curves are the 91-day running means; and the thin curves are the 7-day running means. α=0.92 for the original DPR.

1983; Mathew, 2007). The open water temperature T_W inside the ice pack was chosen as the approximate freezing point. Then, the Arctic sea ice concentration can be retrieved using the original DPR. A series of regions, including the Bering Sea, Chukchi Sea, Barents Sea, and Beaufort Sea, where open water and sea ice were clearly identified in the MODIS, were used to validate and estimate the original DPR algorithm (Zhang et al., 2013). The validation results indicate that the original DPR algorithm can measure reasonable Arctic sea ice concentrations during winter, spring, and autumn. However, the original DPR algorithm retrieved smaller Arctic sea ice concentrations during summer than ABA, NT2, or MODIS. Furthermore, Zhang et al. (2013) did not carry out an in-depth comparison with more traditional algorithms, such as, ABA, NT2, and ASI. The application and comparison of the original DPR algorithm is therefore an important aim of this paper.

2.3 Constant α (α=0.92)

The sea ice area and extent are often taken as climate change indicators in long-term trend analyses and process studies (Zwally et al., 2002; Stroeve et al., 2005). We therefore calculated time series (from June 2002 to August 2011) of Arctic sea ice extent and area from the original DPR, ASI, ABA, and NT2. Figure 2 shows the sea ice extent (bottom) and area (top) time series differences (Note: the values are the difference between DPR and ASI, ABA, or NT2 divide the DPR results.) smoothed with a 91-day running mean (thick blue, red, and black lines) and

Table 2 Mean bias and standard deviations (RMS) between the original DPR and ASI, ABA, and NT2 sea ice extent and area for the AMSR-E period of June 2, 2002 to August 31, 2011

Difference	Sea ice area		Sea ice extent	
	Bias	RMS	Bias	RMS
Original DPR-ASI	-2.1	3.3	-3.6	2.7
Original DPR-ABA	-2.6	3.1	-3.0	1.8
Original DPR-NT2	-2.0	2.3	-1.0	1.1

α=0.92 for the original DPR.

with a 7-day running mean (thin blue, red, and black lines). The 7-day smoothed curves indicate high variability on the scale of a few days, which is the typical time scale of weather systems representing rapidly changing atmospheric influence (Spreen et al., 2008). The 91-day smoothed time series indicates a clear seasonal cycle. The differences between the four algorithms were small during winter, and the largest differences occurred in the summer each year. The differences varied rapidly during spring and autumn. The original DPR and NT2 had the smallest differences in sea ice extent and area.

To compare these four AMSR-E datasets, we used the mean bias and standard deviations (RMS). For the sea ice area: the original DPR minus ASI was -2.1%±3.3%, the original DPR minus ABA was -2.6%±3.1%, and the original DPR minus NT2 was -2.0%±2.3%. For sea ice extent, the differences between the original DPR and ASI, ABA, and NT2 were -3.6%±2.7%, -3.0%±1.8%, and -1.0%±1.1%, respectively. The ± values are given for one standard deviation. These differences are summarized in Table 2. In general, the original DPR results were slightly less than ASI, ABA, and NT2.

At present, we do not know which of the four algorithms best represents Arctic sea ice extent and area. The constant α in the original DPR is also questionable because the maximum difference between the original DPR and ASI, ABA, and NT2 appeared in the summertime. Zhang et al. (2013) also pointed out that the original DPR results were substantially less than MODIS, NT2, or ABA during the summer. Therefore, for applications where not the best representation of the truth but minimal differences between original DPR and other algorithm is worthwhile. Because α is the core of the original DPR, we expect that using a seasonally changing α will decrease the differences between the four algorithms, as will be discussed in Section 2.4.

2.4 Automatic adaption of α

The ratio of the dual-polarized brightness temperature at 36.5 GHz was approximately constant for the 100% ice area during winter; however, its value decreased at the marginal ice zone (MIZ) or in low ice concentration areas (Comiso, 1995; Comiso et al., 2003; Zhang et al., 2013). Figure 3 shows the spatial distribution of the ratio on March 1, 2010. The ratio of dual-polarized brightness temperature changed from 0.73 to 0.92 in a narrow MIZ; however, the ratio changed from 0.92 to 0.96 in a large 100% sea ice area. Therefore, a threshold value should exist when the sea ice concentration is close to 1. Because the ratios of the dual-polarized brightness temperature were higher than the threshold value, the dual-polarized brightness temperature should cluster along line AD (Fig.1). We developed a method to automatically adapt α, improving the DPR ice concentration, especially in summer.

The contrast ratio (CR) is a good parameter to ascertain the edge of two different substances in remote images, such as, sea ice area, sea ice perimeter, and perennial ice extent (Zhao and Ren, 2000). The ratio of vertically to horizontally polarized brightness temperatures at 36.5 GHz is denoted as γ (for 100% sea ice concentration, $\gamma = \frac{\mathrm{TB_H}}{\mathrm{TB_V}} = \frac{\varepsilon_{\mathrm{IH}} T_{\mathrm{I}} C}{\varepsilon_{\mathrm{IV}} T_{\mathrm{I}} C} = \frac{\varepsilon_{\mathrm{IH}}}{\varepsilon_{\mathrm{IV}}} = \alpha$). First, we counted the grid numbers in the whole Arctic region (i.e., $\phi(\gamma)$) for each γ from 0.600 to 0.970. Second, we calculated the differences in each γ between neighboring grids. If the absolute value of a difference was greater than a threshold value P, we counted the grid numbers (i.e., $\delta(\gamma)$). The value of P was set equal to 0.005. Next, CR was defined as

$$\lambda(\gamma)=\delta(\gamma)/\phi(\gamma),$$

$$\gamma\in[0.600,\ 0.601,\ \cdots,\ 0.969,\ 0.970]. \quad (5)$$

This computation process is demonstrated in Fig.4. The red grids represent the 100% sea ice regions and the blue grids represent combination regions of sea ice and open water. When P=0.005 and γ=0.922, the total count of grid numbers in the figure was 10 (ϕ(0.922)=10) and the differences between neighboring grids greater than 0.005 was 8 (δ(0.922)=8). Therefore, the CR of 0.922 was 0.80 (λ(0.922)=8/10=0.80).

Figure 5 shows CR and its γ gradient over the whole Arctic region with different values of P. These two pictures indicate that the values of P only changed the shape of the contrast ratio, but the position of extreme values for gamma were not affected. We therefore used P=0.005. CR clearly decreased when γ

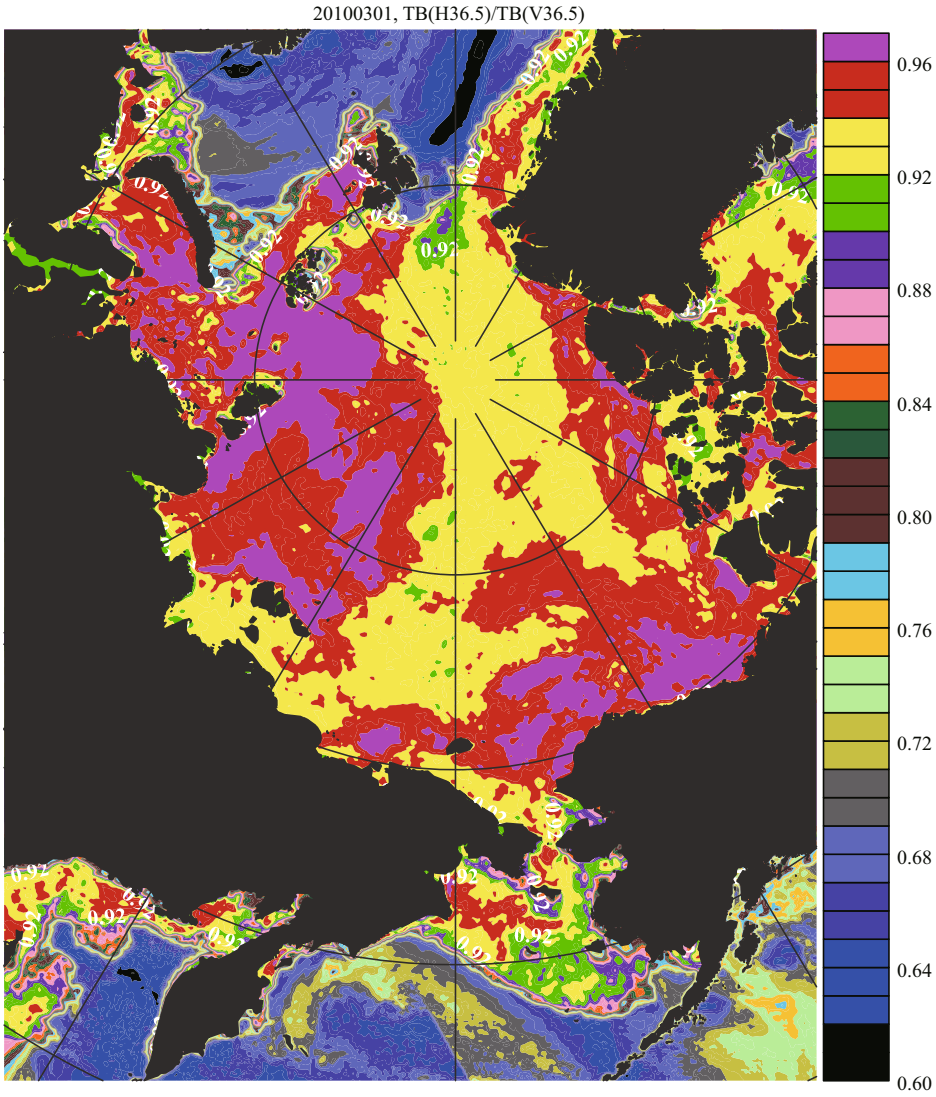

Fig.3 Ratio map of the dual-polarized brightness temperature at 36.5 GHz on March 1, 2010

changed from 0.85 to 0.93 in Fig.5a. The gradient of CR had a minimum value when γ equaled 0.92 in Fig.5b. In the spatial distribution of γ (Fig.3), it changed relatively little in the large Arctic region for the 100% ice concentration. Figure 1 also shows that the dual-polarized brightness temperature at 36.5 GHz clustered to line AD when γ was greater than 0.92. This indicates that the sea ice concentration was nearly 100%. Based on Eq.4, all features indicate that γ was equal to α when γ was greater than 0.92. Therefore, CR and its gradient can be adopted to determine α from the ratio of the dual-polarized brightness temperature at 36.5 GHz.

On the basis of CR and its gradient, the α adaptation was carried out from 2002 to 2011. Running mean curves (91-day) and monthly means of α for the 10 year period are shown in Fig.6. α displayed a seasonal cycle with a period similar to the difference between

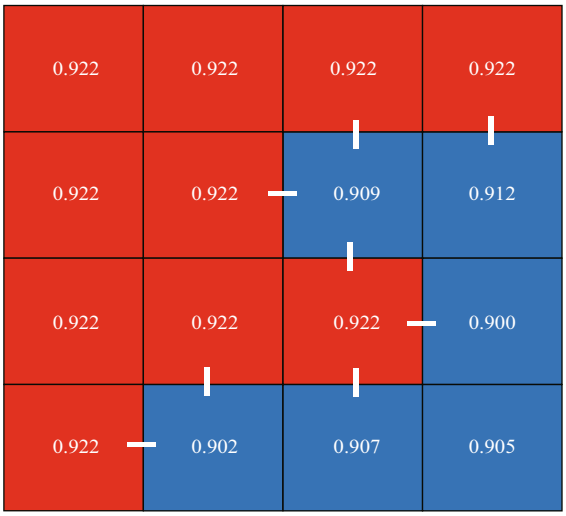

Fig.4 The computation process of CR using the ratio γ

In the plot, the red grids represent the 100% sea ice regions and the blue grids represent combination regions of sea ice and open water.

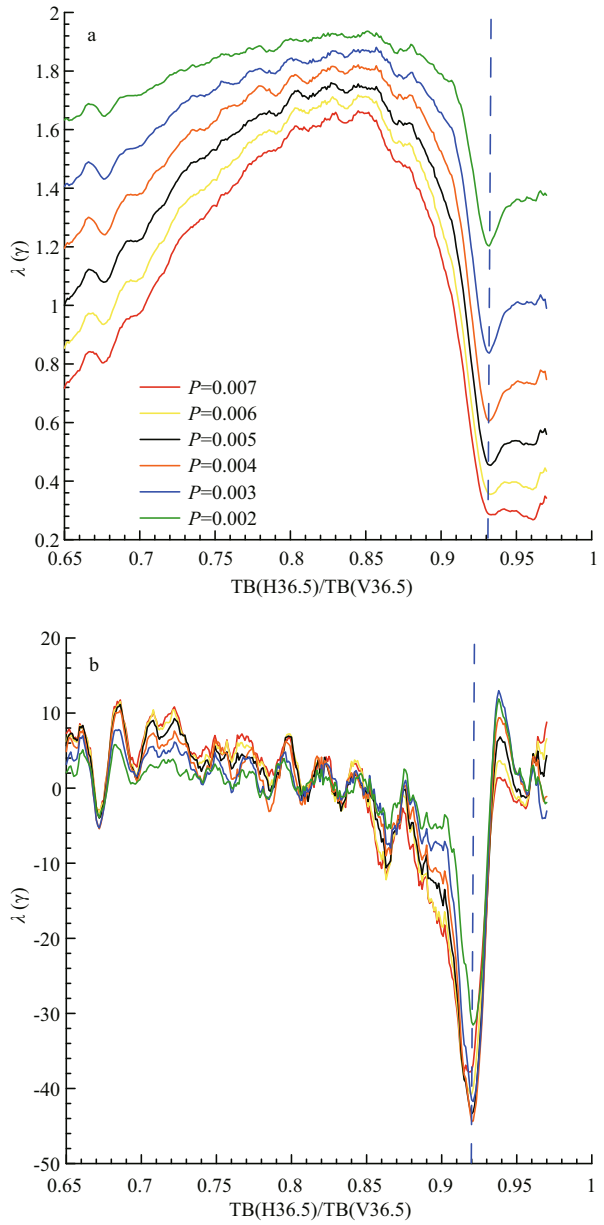

Fig.5 Contrast ratio (a) and its gradient (b) for the dual-polarized brightness temperatures at AMSR-E channel 36.5 GHz on March 1, 2009

Table 3 Mean bias and standard deviations (RMS) between the improved DPR and ASI, ABA, and NT2 sea ice extent and area for the AMSR-E period from June 2, 2002 to August 31, 2011

Difference	Sea ice area		Sea ice extent	
	Bias	RMS	Bias	RMS
Improved DPR-ASI	-0.8	2.0	-3.8	2.8
Improved DPR-ABA	-1.3	1.7	-3.2	1.9
Improved DPR-NT2	-0.7	1.9	-1.3	1.1

α is adapted for the improved DPR.

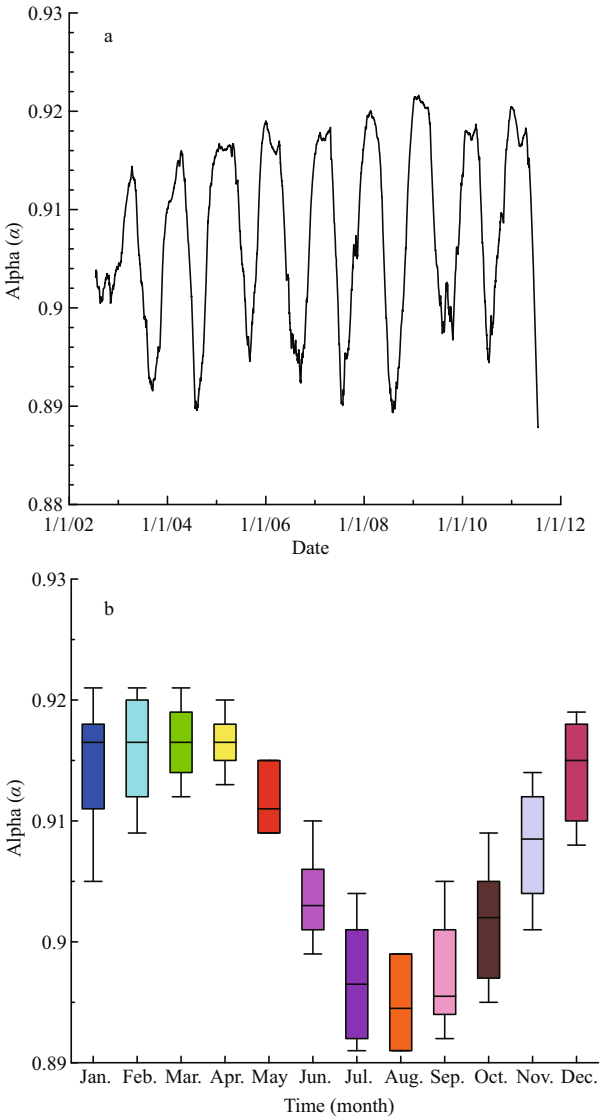

Fig.6 Seasonal development of α based on CR for ten years from 2002 to 2011 (a) and a box plot presenting the ten year monthly means of α (b)

The curve shows the 91-day running mean development of α.

the original DPR, ASI, ABA, and NT2 for the sea ice extent and area (Fig.2). The highest α values occurred in winter, and their value changed slightly (approximately 0.92). However, α varied rapidly in the spring, summer, and autumn; and the smallest α values also occurred in summer.

This method of α adaptation can be operationally implemented; therefore, it can be used in the improved DPR to obtain the Arctic sea ice concentration. When α represented seasonal values, the differences in the sea ice area between the improved DPR and ASI, ABA, and NT2 were -0.8%±2.0%, -1.3%±1.7%, and -1.0%±1.1%, respectively. These differences are summarized in Table 3. According to Tables 2 and 3,

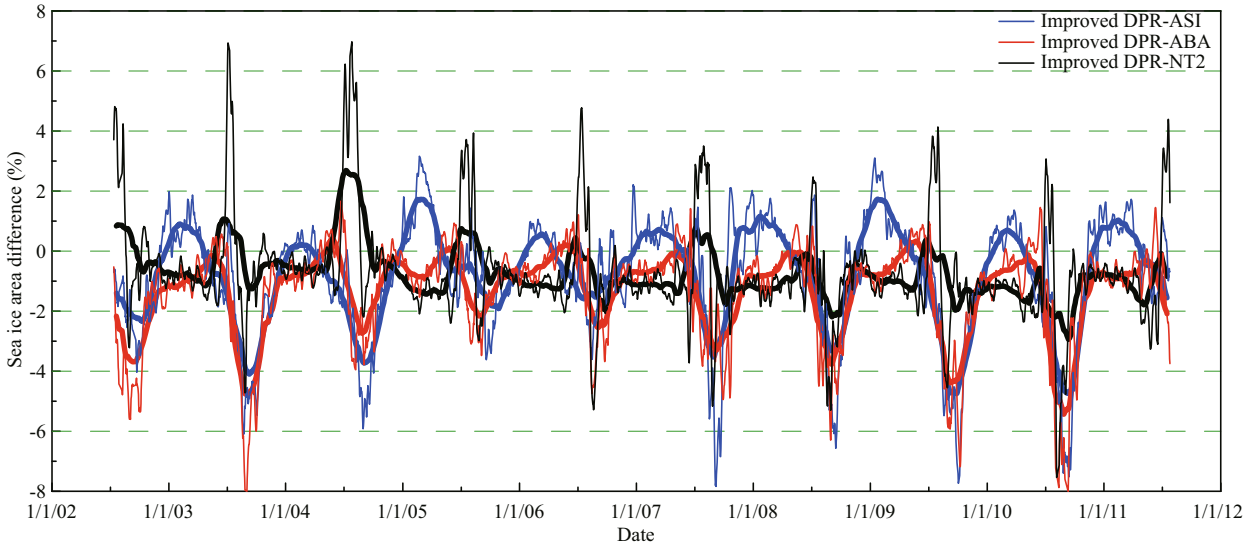

Fig.7 Time series of the differences in the Arctic sea ice area

The thick curves are the 91-day running means; and the thin curves are the 7-day running means. α is adapted for the improved DPR.

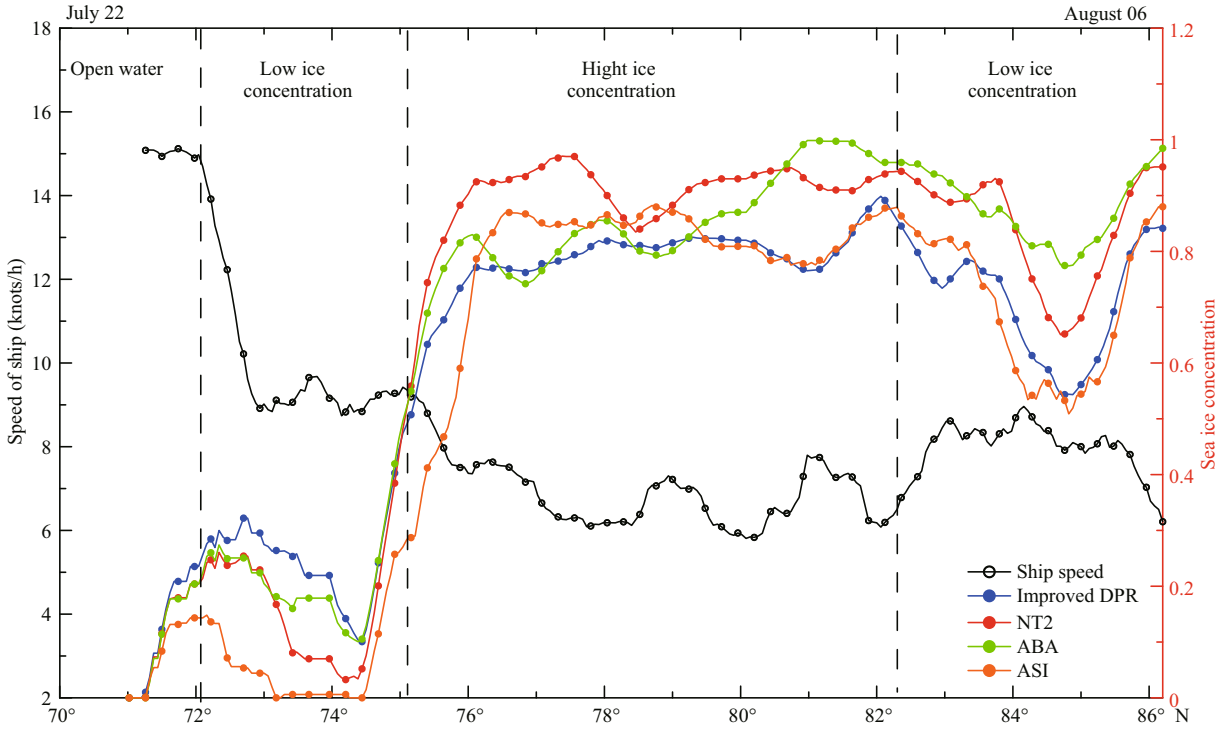

Fig.8 Comparison of four AMSR-E ice concentration algorithms with the speed of the R/V *Xuelong* from July 22 to August 6, 2010

The results of the improved DPR, NT2, ABA, and ASI algorithm ice concentrations are shown as blue, red, green, and orange curves, respectively. The speed of the R/V *Xuelong* is shown as a black curve.

the differences in the sea ice area decreased significantly. Figure 7 shows a time series of sea ice area differences smoothed with a 91-day running mean (thick blue: improved DPR-ASI; red: improved DPR-ABA; and black; improved DPR-NT2 lines) and with a 7-day running mean (thin blue, red, and black lines). According to Figs.3 and 8, only small seasonal differences occurred between the improved DPR and ASI (or ABA). There were also no seasonal differences between the improved DPR and NT2, except in the summer.

In summary, CR provided an adapted α, which improved the DPR results, to calculate the Arctic sea ice concentration. Compared with a constant α in the

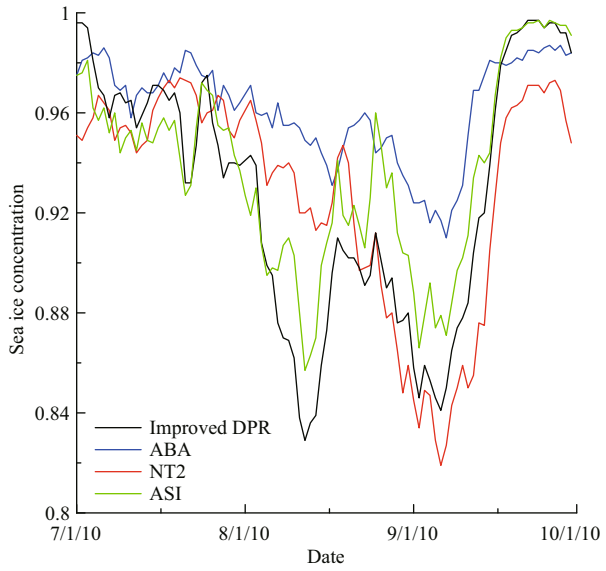

Fig.9 Daily average sea ice concentration from July 1 to September 30, 2010 in the central Arctic (north of 83°N) obtained using four algorithms

Improved DPR (black), ABA (blue), NT2 (red), and ASI (green). α is seasonal for the improved DPR.

original DPR, the differences in the Arctic sea ice area between the improved DPR and ASI (or ABA and NT2) decreased.

3 RESULT AND DISCUSSION

To compare our results to actual, and other, ice concentration fields, we qualitatively used observations of extremely low ice concentrations from the Pacific sector of the central Arctic (north of 83°N) around August 12, 2010. The Chinese National Arctic Research Expedition (CHINARE-2010) surveyed this phenomenon. We also selected MODIS images for four days (July 22, 23, 24, and 28, 2010) from the Beaufort Sea. The choice of these images was restricted by the occurrence of clear days to eliminate the influence of clouds.

3.1 Comparison with ship observations

During CHINARE-2010, the R/V *Xuelong* sailed northward from 153°33.12′W, 72°42.04′N. After ten days, on August 6, the ship arrived at 176°05.88′W, 86°04.85′N. At this location, a long-term ice station was established to observe air-ice-ocean interactions for twelve days (August 7–19).

The sea ice concentration in the Pacific sector of the central Arctic was qualitatively identified by ship speed, which was calculated by GPS data, because the ship navigates with maximum power in different ice conditions. Figure 8 shows the results of four ice concentration algorithms and the speed of the R/V *Xuelong* from July 22 to August 6. It is clear that the ship passed through an area of low sea ice concentration and a first year ice zone from 72.0°N to 75.2°N under an average speed of 9 knots. The average ship speed decreased to 6 knots from 75.2°N to 82.3°N, which was a large area of high ice concentration. From 82.3°N, sea ice concentration decreased rapidly and large areas of open water appeared frequently. The ship speed remained at 8 knots until arriving at the ice camp located at 86°04.85′N. These observations show that there was an extremely low ice concentration in the Pacific sector of the central Arctic (82.3°N). These ice distribution features are supported by a study comparing ship-based visual observations of sea ice concentration and AMSR-E sea ice concentration in Fig.5a of Xie et al. (2013): on the one hand, the ship speed in the lower ice concentration zone were faster than the higher ice concentration zone; on the other hand, ship-based visual observation found a lower ice concentration zone in 83°–86°N.

During CHINARE-2010, we also qualitatively observed the sea ice distribution from a long-term ice station (176°05.88′W, 86°04.85′N) to the North Pole by helicopter (Huang et al., 2016) and found a large area of open water extending from the long-term ice station to the North Pole. Therefore, extremely low ice concentrations occurred in the central Arctic in August, 2010. Figure 9 shows the total sea ice concentration north of 83°N calculated using the four algorithms from July 1 to September 30, 2010. The results of the improved DPR and ASI clearly produced an extremely low ice concentration for August 12 and September 7, and the sea ice concentration increased to a maximum around August 18. However, the extremely low ice concentration only appeared on September 7 for ABA and NT2.

Figure 10 shows the Arctic sea ice concentration maps for August 6, August 12, August 18, and September 7, 2010, obtained using four algorithms (improved DPR, ASI, ABA, and NT2). The black line in each map is the navigation trajectory of R/V *Xuelong* from July 26 to August 6, 2010. Compared with ABA and NT2, the improved DPR results and ASI showed a clear ice zone with low sea ice concentrations in the Pacific sector of the central Arctic in early August. On August 12, in particular, the sea ice concentration along the trajectories of R/V *Xuelong* decreased to 0.5 (or less) in some places

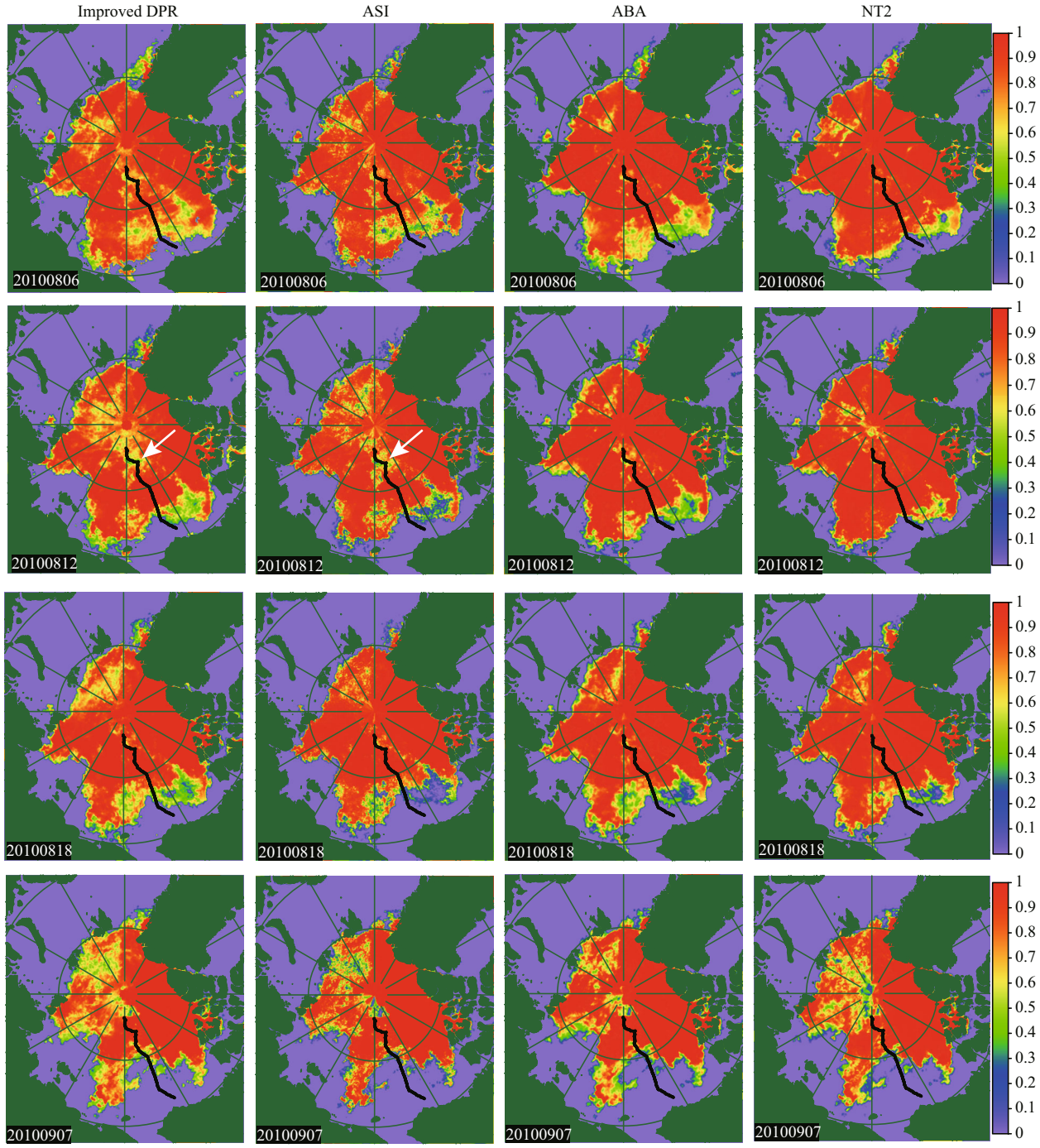

Fig.10 Arctic sea ice concentration maps for August 6, August 12, August 18, and September 7, 2010, obtained from AMSR-E data using four different sea ice concentration algorithms: improved DPR, ASI, ABA, and NT2

The black lines are the navigation trajectories of R/V *Xuelong* from July 26 to August 6, 2010. The white arrow is a location with low ice concentration (or a large area of open water). α is seasonal for the improved DPR.

(such as, the location labeled with a white arrow). The ice zone with low sea ice concentrations also expanded to the North Pole according to the improved DPR and ASI. The results of the improved DPR and ASI were similar and in agreement with the qualitative observations, showing an ice zone with low sea ice concentrations in the Pacific sector of the central Arctic. All algorithms recorded extremely low ice concentrations in the Atlantic sector of the central Arctic around September 7, 2010.

Similar to ASI, ABA, and NT2, the improved DPR also provided reasonable Arctic sea ice concentrations to guide vessel navigation, for example, for the R/V *Xuelong*. In addition, although the improved DPR and

ASI gridded products were 12.5×12.5 km^2 and 6.25×6.25 km^2, respectively, they produced the same sea ice status in the central Arctic.

3.2 Comparison with MODIS data

To assess and compare the four algorithms, the higher resolution (250×250 m^2) MODIS image subsets across the Beaufort Sea on July 22, 23, 24, and 27, 2010 were analyzed. In Fig.11, the MODIS images are located in the first row. The next five rows are sea ice concentration maps in the red frame calculated using MODIS, the improved DPR, ASI, ABA, and NT2. The final row is the comparison of the five sea ice concentration algorithms along the section shown in the figure. Each 12.5×12.5 km^2 grid is composed of 2 500 MODIS pixels. Therefore, the sea ice concentration for each grid is the percentage of ice pixels among the 2 500 MODIS pixels (Zhao and Ren, 2000; Zhang et al., 2013). In general, the spatial distributions of sea ice concentration calculated using the five different methods were similar. Comparing the sections in Fig.11 indicates that the

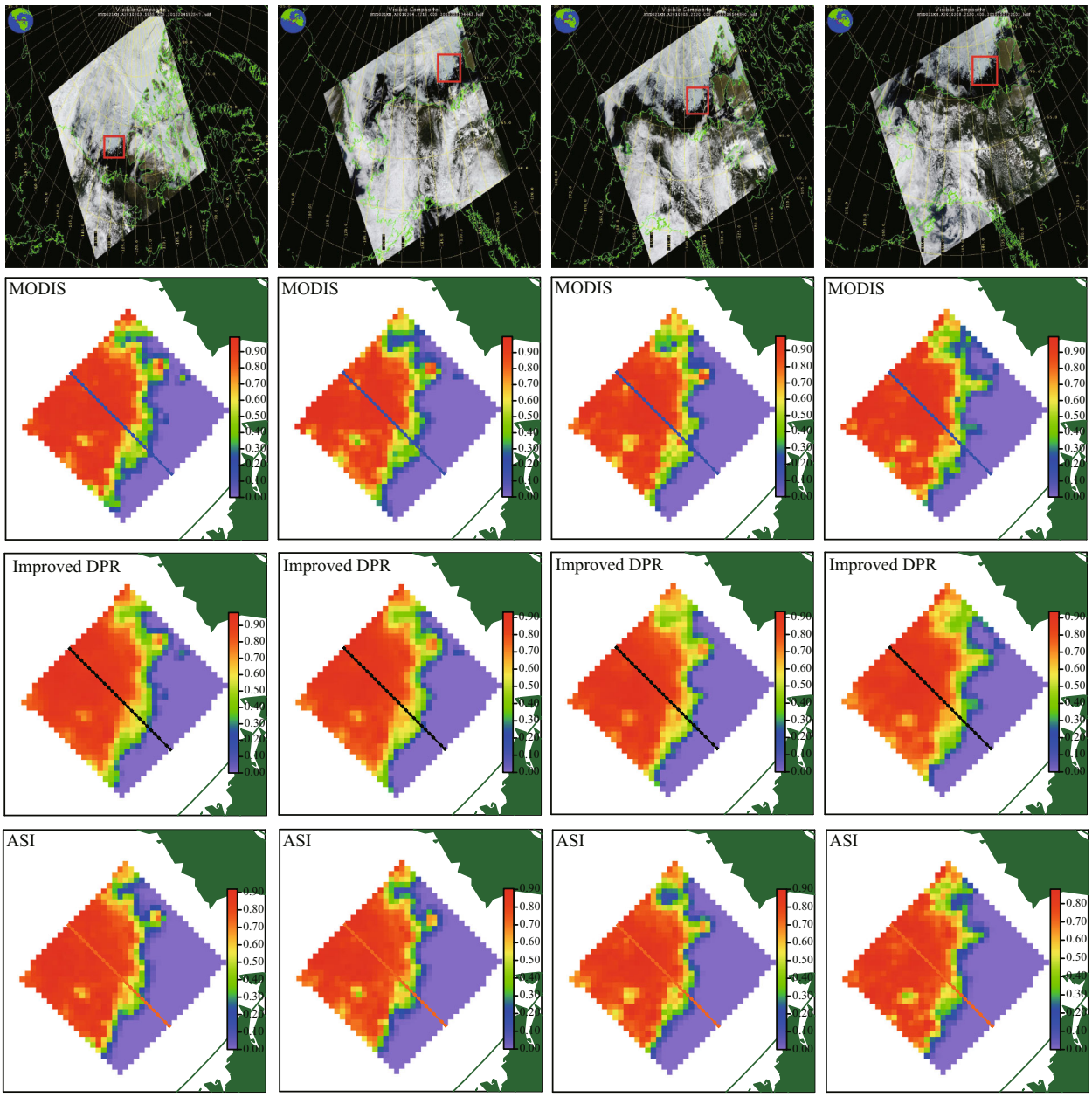

Fig.11 The first row shows MODIS images across the Beaufort Sea on July 22, 23, 24, and 27, 2010

The next five rows are sea ice concentration maps with the red frame calculated using MODIS, improved DPR, ASI, ABA, and NT2. The final row is a comparison of the five sea ice concentration algorithms along one section: MODIS (blue), improved DPR (black), ASI (orange), ABA (red), and NT2 (green). α is seasonal for the improved DPR.

To be continued

Fig.11 Continued

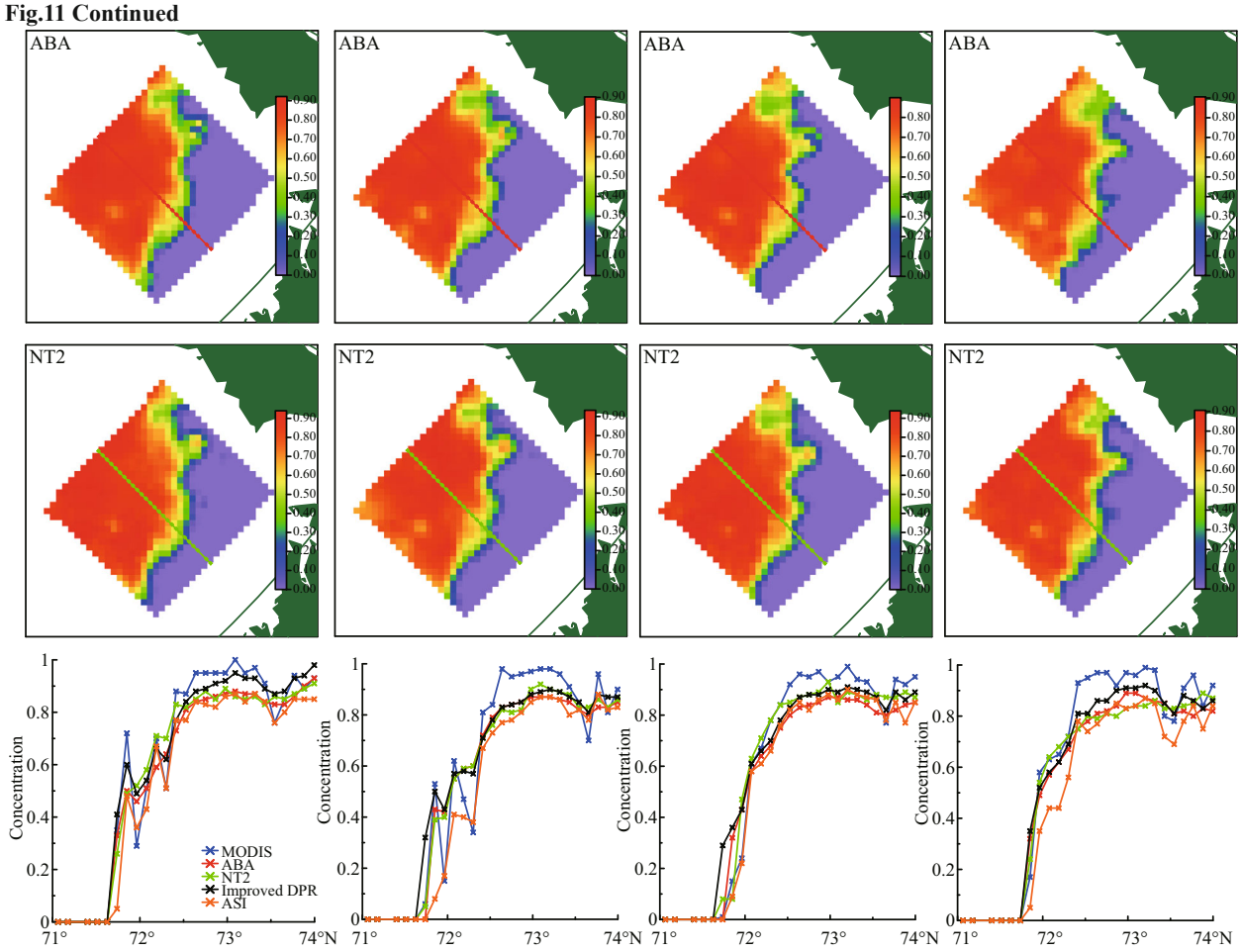

Table 4 Mean bias and standard deviations (RMS) between MODIS and the improved DPR, ASI, ABA, and NT2 sea ice concentration in Fig.11

Difference	22 July		23 July		24 July		27 July	
	Bias	RMS	Bias	RMS	Bias	RMS	Bias	RMS
Improved DPR-MODIS	-0.22	8.13	-0.76	11.34	-5.78	19.29	-2.47	9.05
ASI-MODIS	-7.26	8.77	-7.21	9.46	-11.77	17.86	-9.35	9.62
ABA-MODIS	-3.99	10.31	-2.70	11.60	-8.29	19.29	-5.18	10.35
NT2-MODIS	-2.68	10.01	-1.47	12.04	-6.23	19.50	-2.83	10.74

α is seasonal for the improved DPR.

results of the improved DPR, ASI, ABA, and NT2 were similar in the high-concentration regime and were all less than the MODIS results. Part of this difference may be explained by the relatively higher and less variable sea ice concentration of MODIS that tend to limit errors owing to smearing and atmospheric influences. In addition, we also observed that ASI provided relatively low variability and displayed medium- and low-concentration regimes, where atmospheric influences were predominant.

To quantify the differences between MODIS and other algorithms, the statistics from all grids in Fig.11 are presented in Table 4. All algorithms had negative biases on the four days. This indicates that the results of the four algorithms were influenced by melt ponds, and weather and/or surface conditions of sea ice (Andersen et al., 2007). Table 4 shows that the improved DPR results agreed better with MODIS than the other algorithms and that ASI produced the largest differences. Reasons for this difference

include: 1) ABA and NT2 calculated the sea ice concentration using V18.7 GHz and V36.5 GHz, which have different footprint sizes (V18.7: 16×27 km^2 and V36.5: 8.2×14.4 km^2); and 2) in general, the high-frequency (such as, 89 GHz) channels, which were used in ASI, are highly influenced by weather (Andersen et al., 2007; Spreen et al., 2008). However, the improved DPR only uses H and V36.5 GHz channels to calculate the Arctic sea ice concentration. The footprint size of H and V 36.5 GHz is less than V18.7, and the H and V36.5 GHz data are influenced less by weather than H and V89.0 GHz data.

According to the brightness temperature equations, the improved DPR algorithm uses the 36.5 GHz channels of AMSR-E to retrieve the Arctic sea ice concentration. It also includes an adapted method for the key parameter (α) determination. When the set of α was adapted seasonally, the improved DPR algorithm indicated reasonable results not only in winter, but also in summer. The improved DPR algorithm performed equally well with the other three sea ice concentration algorithms.

4 SUMMARY AND CONCLUSION

The original DPR algorithm uses a fixed coefficient to retrieve Arctic sea ice concentration between 0% and 100%. Results from the comparison to original DPR algorithm and other three passive microwave sea ice concentration algorithms, are seasonally different to the Arctic sea ice extent and area. Recalling that the alpha (α) in original DPR algorithm are more sensitive to radiometric properties, which would change during melting time and refreezing time. Therefore, it is very important to reduce the differences according to appropriate method. For ABA and NT2 algorithms, there have different tie-points during summer and winter (Markus and Cavalieri, 2000). For example, sea ice temperature of the emitting surface is 268K at summer, however it is 248K at winter; Open water temperature of the emitting surface is 274K at summer, however it is 271K at winter. For ASI algorithms, Spreen et al. (2008) provided two priori seasonal coefficients to reduce differences between algorithms during the summer and winter.

In this paper, a new method to determine the α and improve the DPR algorithm has been developed. Using this method, we can easily and automatically constructed a seasonal changes of α in Arctic between 2002 to 2011. Then, we presented results from an inter-comparison of four passive microwave sea ice concentration algorithms (including improved DPR, ASI, ABA and NT2) and a comparison with ship-based observations. At last, under clear sky conditions, MODIS imagery was used to generate high resolution sea ice concentration datasets with which to assess AMSR-E ice concentration retrievals for four days in July 2010. In general, our comparisons showed that the improved DPR performed with similar quality as the other three sea ice algorithms. Specific conclusions are as follows.

Analysis of the entire AMSR-E time series for the Arctic showed differences between the original DPR for constant α (α=0.92) and ASI. ABA and NT2 had significant seasonal cycles, both in ice extent and areal estimates, which were more pronounced during summer. In general, the original DPR and ASI had the largest differences in sea ice extent, whereas DPR and ABA had the largest differences in sea ice area. In addition, the original DPR and NT2 had the smallest differences in ice extent and areal estimates.

The CR for dual-polarized brightness temperatures at 36.5 GHz provided a seasonal α to improve DPR. Our study indicates that the seasonal α changed slowly during winter, and rapidly during other times, and reached its minimum during summer. Systematic differences in the Arctic sea ice area using the four algorithms suggest that the improved DPR and NT2 were almost identical, except in summer. However, the improved DPR and ABA (or ASI) also had small seasonal cycle differences. Differences in sea ice area between DPR and ASI, ABA, and NT2 were reduced from -2.1%±3.3%, 2.6%±3.1%, and -2.0%±2.3% (α was constant at 0.92) to -0.8%±2.0%, 1.3%±1.7%, and -0.7%±1.9% (α with a seasonal cycle), respectively. This result suggests that the improved DPR provides a more reasonable data product than the original DPR with a constant α.

Results from the comparison with ship-based observations and MODIS-based concentrations indicate that the improved DPR and ASI were in good agreement with extremely low ice concentrations that occurred in the Pacific sector of the central Arctic (north of 83°N) around August 12, 2010, as surveyed by CHINARE-2010. According to the mean bias and standard deviations (RMS), the improved DPR provided a minimum value, followed by NT2 and ABA, with the maximum produced by ASI. This means that similar to ASI, ABA, and NT2, the improved DPR also provided a reasonable sea ice concentration value, which can be used for estimates

Table 5 The main datasets applied in this study

Data	Institution	URL
TB for 18.7, 23.8 and 36.5 GHz	NSIDC	http://nsidc.org/data
Sea ice concentration for ABA and NT2	NSIDC	http://nsidc.org/data
Sea ice concentration for ASI	University of Bremen	https://seaice.uni-bremen.de/data
MODIS image data/map	NASA	http://ladsweb.nascom.nasa.gov/

of heat flux in numerical atmospheric and ocean models, polynya size determination, and calculations of ice extent and area time series in climate studies.

5 DATA AVAILABILITY STATEMENT

See Table 5.

6 ACKNOWLEDGEMENT

We also acknowledge the AMSR-E data and the MODIS images provided by the National Snow and Ice Data Center, University of Bremen, and NASA. We thank the sea ice groups and all the crew on R/V Chinese National Arctic Research Expedition (CHINARE-2010) for their observations of sea ice conditions.

We thank Reetta Saikku, PhD, from Liwen Bianji, Edanz Group China (www.liwenbianji.cn/ac), for editing the English text of a draft of this manuscript.

References

Andersen S, Tonboe R, Kaleschke L, Heygster G, Pedersen L T. 2007. Intercomparison of passive microwave sea ice concentration retrievals over the high-concentration Arctic sea ice. *J. Geophys. Res.*, **112**(C8): C08004, https://doi.org/10.1029/2006JC003543.

Comiso J C, Cavalieri D J, Markus T. 2003. Sea ice concentration, ice temperature, and snow depth using AMSR-E Data. *IEEE Transactions on Geoscience and Remote Sensing*, **41**(2): 243-252, https://doi.org/10. 1109/TGRS.2002.808317.

Comiso J C, Zwally H J. 1997. Temperature corrected Bootstrap algorithm. *In*: 1997 IEEE International Geoscience and Remote Sensing, 1997. IGARSS '97. Remote Sensing—A Scientific Vision for Sustainable Development. IEEE, Singapore. p.857-861, https://doi.org/10.1109/IGARSS.1997.615279.

Comiso J C. 1995. SSM/I concentrations using the Bootstrap algorithm. NASA Reference Publication 1380. National Aeronautics and Space Administration, Washington, DC. 49p.

Gloersen P, Cavalieri D J. 1986. Reduction of weather effects in the calculation of sea ice concentration from microwave radiances. *J. Geophys. Res.*, **91**(C3): 3 913-3 919, https://doi.org/10.1029/JC091iC03p03913.

Hebert D A, Allard R A, Metzger E J, Posey P G, Preller R H, Wallcraft A J, Phelps M W, Smedstad O M. 2015. Short-term sea ice forecasting: an assessment of ice concentration and ice drift forecasts using the U.S. Navy's Arctic Cap Nowcast/Forecast System. *J. Geophys. Res.*, **120**(12): 8 327-8 345, https://doi.org/10.1002/2015JC011283.

Huang W, Lu P, Lei R, Xie H, Li Z. 2016. Melt pond distribution and geometry in high Arctic sea ice derived from aerial investigations. *Annals of Glaciology*, **57**(73): 105-118, https://doi.org/10.1017/aog.2016.30.

Liu J P, Curry J A, Martinson D G. 2004. Interpretation of recent Antarctic sea ice variability. *Geophys. Res. Lett.*, **31**(2): L02205, https://doi.org/10.1029/2003GL018732.

Maaβ N, Kaleschke L. 2010. Improving passive microwave sea ice concentration algorithms for coastal areas: applications to the Baltic Sea. *Tellus A*, **62**(4): 393-410, https://doi.org/10.1111/j.1600-0870.2010.00452.x.

Markus T, Cavalieri D J. 2000. An enhancement of the NASA team sea ice algorithm. *IEEE Transactions on Geoscience and Remote Sensing*, **38**(3): 1 387-1 398, https://doi.org/10.1109/36.843033.

Mathew N. 2007. Retrieval of surface emissivity of sea ice and temperature profiles over sea ice from passive microwave radiometers. Ph.D. dissertation, Univ. Bremen, Bremen, Germany.

Nakamura T, Yamazaki K, Iwamoto K, Honda M, Miyoshi Y, Ogawa Y, Tomikawa Y, Ukita J. 2016. The stratospheric pathway for Arctic impacts on midlatitude climate. *Geophys. Res. Lett.*, **43**(7): 3 494-3 501, https://doi.org/10.1002/2016GL068330.

Serreze M C, Stroeve J. 2015. Arctic sea ice trends, variability and implications for seasonal ice forecasting. *Philosophical Transactions of the Royal Society A: Mathematical, Physical and Engineering Sciences*, **373**: 20140159, https://doi.org/10.1098/rsta.2014.0159.

Spreen G, Kaleschke L, Heygster G. 2008. Sea ice remote sensing using AMSR-E 89-GHz channels. *J. Geophys. Res.*, **113**: C02S03, https://doi.org/10.1029/2005JC003384.

Stocker T F, Qin D, Plattner G K, Tignor M M B, Allen S K, Boschung J, Nauels A, Xia Y, Bex V, Midgley P M. 2013. Climate Change 2013: The Physical Science Basis. Working Group 1 Contribution to the Fifth Assessment Report of the Intergovernmental Panel on Climate Change. Cambridge Univ. Press, Cambridge.

Stroeve J C, Crawford A D, Stammerjohn S. 2016. Using timing of ice retreat to predict timing of fall freeze-up in the Arctic. *Geophys. Res. Lett.*, **43**(12): 6 332-6 340, https://doi.org/10.1002/2016GL069314.

Stroeve J C, Serreze M C, Fetterer F, Arbetter T, Meier W, Maslanik J, Knowles K. 2005. Tracking the arctic's shrinking ice cover: another extreme September minimum in 2004. *Geophys*. *Res*. *Lett*., **32**(4): L04501, https://doi.org/10.1029/2004GL021810.

Sumata H, Gerdes R, Kauker F, Karcher M. 2015. Empirical error functions for monthly mean Arctic sea-ice drift. *J*. *Geophys*. *Res*., **120**(11): 7 450-7 475, https://doi.org/10.1002/2015JC011151.

Svendsen E, Kloster K, Farrelly B, Johannessen O M, Johannessen J A, Campbell W J, Gloersen P, Cavalier D J, Mätzler C. 1983. Norwegian remote sensing experiment: evaluation of the nimbus 7 Scanning multichannel microwave radiometer for sea ice research. *J*. *Geophys*. *Res*., **88**(C5): 2 781-2 791, https://doi.org/10.1029/JC088iC05p02781.

Webster M A, Rigor I G, Perovich D K, Rechter-Menge J A, Polashenski C M, Light B. 2015. Seasonal evolution of melt ponds on Arctic sea ice. *J*. *Geophys*. *Res*., **120**(9): 5 968-5 982, https://doi.org/10.1002/2015JC011030.

Xie H, Lei R, Ke C, Wang H, Li Z, Zhao J, Ackley S F. 2013. Summer sea ice characteristics and morphology in the Pacific Arctic Sector as observed during the CHINARE 2010 cruise. *The Cryosphere*, **7**(4): 1 057-1 072, https://doi.org/10.5194/tc-7-1057-2013.

Zhang S G, Zhao J P, Frey K, Su J. 2013. Dual-polarized ratio algorithm for retrieving Arctic sea ice concentration from passive microwave brightness temperature. *Journal of Oceanography*, **69**(2): 215-227, https://doi.org/10.1007/s10872-012-0167-z.

Zhao J P, Ren J P. 2000. Study on the method to analyze parameters of Arctic sea ice from airborne digital imagery. *Journal of Remote Sensing*, **4**(4): 271-278, https://doi.org/10.11834/jrs.20000406.

Zwally H J, Comiso J C, Parkinson C L, Cavalieri D J, Gloersen P. 2002. Variability of Antarctic sea ice 1979-1998. *J*. *Geophys*. *Res*., **107**(C5): 9-1-9-19, https://doi.org/10.1029/2000JC000733.